ELSEVIER

Contents lists available at ScienceDirect

Biomaterials Advances

journal homepage: www.journals.elsevier.com/materials-science-and-engineering-c





Structural properties of optically clear bacterial cellulose produced by *Komagataeibacter hansenii* using arabitol

Elizabeth M. van Zyl^a, Mitchell A. Kennedy^b, Wendy Nason^c, Sawyer J. Fenlon^a, Eric M. Young^d, Luis J. Smith^c, Surita R. Bhatia^b, Jeannine M. Coburn^{a,*}

- ^a Department of Biomedical Engineering, Worcester Polytechnic Institute, Worcester, MA 01609, United States of America
- ^b Department of Chemistry, Stony Brook University, Stony Brook, NY 11794, United States of America
- ^c Carlson School of Chemistry and Biochemistry, Clark University, Worcester, MA 01610, United States of America
- ^d Department of Chemical Engineering, Worcester Polytechnic Institute, Worcester, MA 01609, United States of America

ARTICLE INFO

Keywords: Bacterial cellulose Biomaterials Arabitol Nanostructure Nanofiber Transparency

ABSTRACT

Bacterial cellulose (BC) exhibits beneficial properties for use in biomedical applications but is limited by its lack of tunable transparency capabilities. To overcome this deficiency, a novel method to synthesize transparent BC materials using an alternative carbon source, namely arabitol, was developed. Characterization of the BC pellicles was performed for yield, transparency, surface morphology, and molecular assembly. Transparent BC was produced using mixtures of glucose and arabitol. Zero percent arabitol pellicles exhibited 25% light transmittance, which increased with increasing arabitol concentration through to 75% light transmittance. While transparency increased, overall BC yield was maintained indicating that the altered transparency may be induced on a micro-scale rather than a macro-scale. Significant differences in fiber diameter and the presence of aromatic signatures were observed. Overall, this research outlines methods for producing BC with tunable optical transparency, while also bringing new insight to insoluble components of exopolymers produced by *Komagataeibacter hansenii*.

1. Introduction

Transparent materials are needed in biomedical applications like wound dressing, to monitor healing, and in biosensing, to interface with optical devices. Predominantly produced by *Komagataeibacter* ssp., BC is synthesized and extruded as ribbon-like microfibers that further self-assemble into network-structured pellicles at the air-liquid interface of static liquid cultures [1]. This network structure and BC's composition of $\beta(1 \rightarrow 4)$ linked D-glucose monomer units produces cellulose with inherent biocompatibility, water holding capacity, liquid/gas permeability, and handleability properties [2–4]. However, only a few reports have qualitatively described methods for transparent BC production

[2-6].

The predominant method to induce transparency in BC is through the incorporation of composite materials such as poly(2-hydroxyethyl methacrylate) (PHEMA), poly(methyl methacrylate) (PMMA), poly (ethylene glycol) (PEG), and cyclodextrin [2–7]. PHEMA, commonly used in soft contact lenses, exhibits around 95% light transmittance in its pure form [5]. Di et al. found that, by making a BC/PHEMA composite, the transmittance of native BC can be increased by roughly 10% [5]. Similarly, Kono et al. increased the overall transparency of BC fibers by increasing the concentration of PMMA as a composite material [7]. Though beneficial for increasing transparency, the incorporation of composite materials increases cost and manufacturing time.

Abbreviations: ANOVA, analysis of variance; ATCC, American Type Culture Collection; BC, bacterial-derived cellulose; CP-MAS, Cross-Polarization Magic Angle Spinning; EGF, epidermal growth factor; FBS, Fetal bovine serum; FGF, fibroblast growth factor; HS, Hestrin Schramm; HSD, honest significance test; K., Komagataeibacter; μ_{max} , maximum growth rate; NHDF, normal human dermal fibroblast; NMR, nuclear magnetic resonance spectroscopy; PEG, poly(ethylene glycol); PHEMA, poly(2-hydroxyethyl methacrylate); PMMA, poly(methyl methacrylate); PPP, pentose phosphate pathway; SAXS, Small-angle X-ray scattering; SD, standard deviation; SEM, Scanning electron microscopy; TCP, Tissue culture plastic; WAXS, wide angle X-ray scattering.

^{*} Corresponding author at: Department of Biomedical Engineering, Worcester Polytechnic Institute, 100 Institute Road, Worcester, MA 01609, United States of America.

E-mail addresses: emvanzyl@wpi.edu (E.M. van Zyl), mitchell.kennedy@stonybrook.edu (M.A. Kennedy), WNason@clarku.edu (W. Nason), sjfenlon@wpi.edu (S.J. Fenlon), emyoung@wpi.edu (E.M. Young), LUSmith@clarku.edu (L.J. Smith), surita.bhatia@stonybrook.edu (S.R. Bhatia), jmcoburn@wpi.edu (J.M. Coburn).

Furthermore, synthesis of pure transparent BC would allow for increased use in biomedical applications such as for wound care and biosensing [8].

Utilizing defined minimal culture medium, Souza et al. was able to produce pure transparent BC from *Komagataeibacter hansenii* [9]. It was noted that the transparent material had a lower fiber density compared to cellulose formed in full culture medium. This low fiber density was attributed to nutrient restriction caused by the defined minimal medium. Wang et al. observed similar changes in transparency when creating anisotropic biofilms with aligned BC nanofibers [10]. BC pellicles stretched to 40% strain exhibited increased light transmittance properties when compared to unstretched pellicles [11]. These findings suggest that altering the morphology and hierarchical structure of the cellulose fibers may alter the optical properties of the material. These findings further point to media formulation, specifically nutrient restriction in defined medium, as a possible way to control morphology and structure of BC.

Several studies have investigated media formulation for its impact on BC production and yield. These focus largely on different carbon sources and associated concentrations. Specifically, pure hexose and hexosederived polyol sugars, such as glucose, fructose, and mannitol, allow for higher cellulose production, while pentose and pentose-derived polyol sugars, such as xylose, xylitol, and arabitol, result in decreased cellulose production [12,13]. Additionally, BC has been effectively produced using complex media like waste fruit juice, orange peels, molasses, cheese whey, and other industrial/food waste sources [14–16]. These waste resources are generally rich in mixtures of hexose sugars such as glucose and fructose, and typically result in high cellulose production [17].

Besides changes in overall cellulose production, differences in cellulose hierarchical structure, notably the crystallinity, have been observed when comparing hexose and pentose carbon sources [18,19]. Keshk and Sameshima determined that the use of glucose produced cellulose with 88% crystallinity, while pentose and pentose-derived sugars such as arabitol and xylose produced cellulose with a degree of crystallinity as low as 75% [18,19]. While altered transparency was not reported in these studies, it is generally understood that polymer matrices become more opaque with increasing crystallinity [20].

The mechanism by which this altered crystallinity occurs is not fully understood but it is believed to be due to differences in the metabolic pathways of specific hexose and pentose sugars [19,21,22]. Since BC is made from uridine diphosphate-glucose monomers, it is thought that hexose and hexose-derived sugars like glucose, fructose, and mannitol can readily be converted to BC monomers [23]. This would explain the high BC production on these sugars [24]. However, pentose and pentose-derived sugars, such as arabitol and xylose, are metabolized through the pentose phosphate pathway (PPP), which means that bacteria cultured with pentose sugars as a carbon source must instead use the gluconeogenesis pathway to synthesize BC monomers [19,23]. This increased energetic cost likely results in the observed low BC production from pentose sugars.

Based on the likely connection between carbon source metabolism, BC structure, and transparency, we investigated and characterized BC pellicles produced using different ratios of hexose and pentose sugar mixtures. We chose, the pentose sugar, arabitol, because of its impact on the PPP under certain conditions, as shown by Oikawa et al. [19]. Blends of arabitol and glucose with a constant total carbon source molarity were investigated. The objective was to determine the relationship between cellulose transparency and molecular level properties to gain an understanding of the transparency. The bacterial growth rates, BC yield, transparency, morphology, and hierarchical chemical structure of BC formed were evaluated.

2. Materials and methods

2.1. Materials

Komagataeibacter hansenii NQ5 (K. hansenii ATCC 53582) was purchased from the American Type Culture Collection (ATCC), Manassas, VA, USA. Bacto $^{\text{TM}}$ peptone and Difco $^{\text{TM}}$ yeast extract was purchased from Becton, Dickenson and Company, Franklin Lakes, NJ, USA, while agar was sourced from Sunrise Science Products, San Diego, CA, USA. Darabitol (>99% purity), and sodium chloride (ACS reagent, ≥99% purity) were purchased from Alfa Aesar Co., Inc., China. D-glucose (Bio-Reagent, ≥99.5% purity), citric acid (99% purity), sodium phosphate dibasic (BioReagent, ≥99.5% purity), sodium hydroxide (ACS reagent, ≥97.0% purity), calcium chloride (≥93% purity), and cellulase from *Trichoderma reesei* (aqueous solution, >700 units/g) were sourced from Sigma-Aldrich, Burlington, MA, USA. Iscove's modified Dulbecco's medium was purchased from Lonza Biologics, Walkersville, MD, USA, while fetal bovine serum (FBS), 0.25% trypsin-EDTA, penicillin streptomycin, and 200 mM L-glutamine were sourced from Life Technologies, Waltham, MA, USA. Animal-free recombinant human epidermal growth factor (EGF) and fibroblast growth factor (FGF) were purchased from PeproTech, Waltham, MA, USA. Tris buffered saline (TBS) was sourced from VWR Life Sciences, Bridgeport, NJ, USA. All well plates were sourced from Greiner Bio-One, Monroe, NC, USA, and Falcon™ roundbottom test tubes were sourced from Corning, Inc., Corning, NY, USA.

2.2. BC pellicle production and purification

The cellulose-producing bacterial strain, Komagataeibacter hansenii NQ5 was streaked onto a Hestrin Schramm (HS) agar plate (20 mg/mL glucose, 5 mg/mL peptone, 5 mg/mL veast extract, 1.15 mg/mL citric acid, 2.7 mg/mL disodium phosphate, 15 mg/mL agar) and allowed to grow at 30 °C for 4 d. Single colonies from the HS plate were used to inoculate 5 mL of HS liquid medium (20 mg/mL glucose, 5 mg/mL peptone, 5 mg/mL yeast extract, 1.15 mg/mL citric acid, 2.7 mg/mL disodium phosphate) in a 14 mL Falcon™ round bottom culture tube and allowed to grow on a rotating drum for 4 d at 30 $^{\circ}$ C. The culture was then expanded in static cultures using 10% (v/v) inoculum in fresh HS medium. Fresh HS medium without a carbon source was then inoculated with 0.1% (v/v) static cultured bacteria and supplemented to 1 mM of total carbon source. To allow for pellicle formation, 2 mL of inoculated HS media, was cultured in 12-well tissue culture plates under static conditions at 30 $^{\circ}\text{C}$ for 7 d. To purify the BC pellicles, they were removed, washed in 0.1 M NaOH at 60 $^{\circ}\text{C}$ for 4 h, and then rinsed with DI H₂O until the fluid reached a neutral pH.

2.3. Cellulose yield

To determine the effects of varying concentrations of glucose and arabitol as a carbon source, fresh HS medium without a carbon source was inoculated with 0.1% (v/v) static cultured bacteria. The media was

Table 1Arabitol and glucose concentrations used for bacteria growth and BC production.

Label	Arabitol concentration (mM)	Glucose concentration (mM)
100% arabitol	1.00	0.00
95% arabitol	0.95	0.05
90% arabitol	0.90	0.10
85% arabitol	0.85	0.15
80% arabitol	0.80	0.20
75% arabitol	0.75	0.25
50% arabitol	0.50	0.50
25% arabitol	0.25	0.75
0% arabitol	0.00	1.00

supplemented to 1 mM of total carbon source with mixtures of p-arabitol and p-glucose (Table 1). From here on, the arabitol/glucose combination will be reported as per the given label and referred to as the "arabitol concentration."

Pellicles were allowed to form and were purified using the methods described above. Purified pellicles were weighed while hydrated and then lyophilized using a shelf lyophilizer (Labconco, Kansas City, MO) for 48 h at a temperature of $-25\,^{\circ}\mathrm{C}$ and an absolute vacuum pressure of 0.210 Torr. Estimated BC pellicle thickness was calculated using the hydrated weight and Eq. (1):

$$volume = \frac{mass}{density} \tag{1}$$

where mass refers to the hydrated BC pellicle weight and density refers to the reported hydrated cellulose density of 1.25 g cm $^{-3}$ [25]. In this case, the volume refers to that of a cylinder, $\pi r^2 h$, where r is the radius of a well in a 12-well plate, and h refers to pellicle thickness. Estimated BC pellicle thickness was determined by solving for h. Sideview images were also taken to qualitatively compare the thickness of the pellicles. After lyophilized pellicles were weighed, and the bacterial cellulose yield was calculated using Eq. (2).

% yield =
$$\frac{cellulose\ dry\ weight}{total\ carbon\ source\ weight} \times 100$$
 (2)

The total carbon source mass was calculated using the molar concentrations, the molecular masses, and the total volumes of all carbon sources in culture.

2.4. Bacterial growth kinetics

Growth kinetic studies were performed to identify the effects of arabitol concentration on the growth rate of *K. hansenii*. In a 96-well plate, inoculated HS media was supplemented with 0.4% (v/v) cellulase from *Trichoderma reesei*. The media was supplemented with the carbon sources (Table 1). Absorbance measurements at 600 nm were taken every 30 m for 7 d under shaken conditions at 30 °C (Biotek Synergy H1, Winooski, VT). The maximum growth rate (μ_{max}) was identified from the slope of the linear region of the kinetic curves (Fig. S1).

2.5. Light transmission analysis

The light transmission of freshly produced BC pellicles was measured in the visible light region using a UV–Vis spectrophotometer (Thermo Scientific Evolution 300 UV–Visible Spectrophotometer, Waltham, MA). All transmissions readings were performed inside the enclosed UV–Vis spectrophotometer chamber, to prevent light reflection from outside sources. Transmission spectral readings were performed between wavelengths of 300–800 nm with a step size of 2 nm. Average visible light transmission (400–700 nm range) was compared between test groups. Using this method, light transmission measurements of a commercially available transparent hydrogel wound dressing (CovidienTM KendallTM, Mansfield, MA) were also performed.

2.6. Liquid absorption

The liquid absorption capabilities of BC pellicles were assessed in a salt solution containing 142 mM sodium chloride and 3.3 mM calcium chloride in de-ionized water. The salt solution was prewarmed to 37 $^{\circ}$ C. Lyophilized BC pellicles were weighed and placed in the salt solution weighing a minimum of 40-times that of the lyophilized BC pellicles and incubated at 37 $^{\circ}$ C. Pellicles were weighed at 1 h and 24 h after initial submersion in the salt solution. Liquid absorbance was then calculated relative to the dry material weight.

2.7. Cytotoxicity analysis

Cytotoxicity studies were performed to determine if the BC pellicles produced using different carbon source mixtures impact overall material biocompatibility. BC pellicles produced using 85% and 0% arabitol was used to compare cytotoxicity. BC pellicles were formed in 96-well plates and purified as described above, then autoclaved in $1\times$ tris-buffered saline (TBS; 25 mM tris, 140 mM NaCl, 3 mM KCl, pH 7.2). Normal Human Dermal Fibroblasts (NHDF; American Type Culture Collection CRL-2565) were cultured in growth medium (Iscove's modified Dulbecco's medium, 10% FBS, 100 U/mL penicillin, 100 μ g/mL streptomycin, 2 mM $_L$ -glutamine, 0.01 $\mu g/mL$ EGF, 0.005 $\mu g/mL$ FGF) at 37 $^{\circ}C$ and 5% CO₂. Cells were passaged serially using 0.25% trypsin-EDTA. For cytotoxicity studies, wells in 48-well plates were seeded with 3000 NHDF and the cells allowed to attach for 24 h. BC pellicles were then placed in cell seeded wells. Three days after adding BC pellicles, a resazurin metabolic assay was performed to quantify cell metabolism. Fluorescent signal of the resazurin solution after incubation were read at an excitation wavelength of 544 nm and emission wavelength of 590 nm using a SpectraMax M2 plate reader (Molecular Devices Inc., San Jose, CA). Cells were also cultured on tissue culture plastic (TCP) with no BC pellicles added as an untreated control, and resazurin solution was added to wells with no cells as a background control. Results were normalized to the untreated control measurements.

2.8. Scanning electron microscopy (SEM) and image analysis

The morphology of BC pellicles produced using 100%, 85%, 50%, and 0% arabitol concentration was evaluated to identify difference in cellulose fiber diameter. Pellicles were dried overnight, sputter coated with two coats of 4 nm of gold (Sputter Coater Cressinton 208HR, Watford, England) and imaged with a field emission scanning electron microscope using an 8–10 kV electron beam (Quanta 200 FEG MK11, FEI Inc., Hillsboro, Oregon). Images were taken at $30,000\times$ and fiber diameter was analyzed manually using ImageJ, where a minimum of 200 fibers were analyzed per image.

2.9. Small-angle X-ray scattering (SAXS) and wide-angle X-ray scattering (WAXS)

Pellicles for small-angle scattering (SAXS) and wide-angle X-ray scattering (WAXS) were loaded into 1.0-mm glass thin-walled capillaries (Charles Supper, Westborough, MA). SAXS and WAXS measurements were conducted at the Complex Materials Scattering (CMS, 11-BM) beamline of the National Synchrotron Light Source II (NSLS-II) at Brookhaven National Laboratory. The scattered data were collected using a beam energy of 13.5 keV and beam size of 200 \times 200 μm with a Pilatus 2 M area detector (Dectris, Switzerland). For SAXS studies, the detector, consisting of 0.172 mm square pixels in a 1475 \times 1679 array, was placed five meters downstream from the sample position. The collected 2D scattering patterns were reduced to 1D scattering intensity, I(q), by circular average, where q is the magnitude of the scattering vector, $q = (4\pi/\lambda) \sin(\theta)$, where λ is the wavelength of the incident X-ray beam, 0.9184 Å, and 2θ is the scattering angle. For SAXS studies, the qrange measured was 0.0034-0.185 A⁻¹. A blank of glass and air was subtracted from the original data for further analysis. Crystallite sizes were estimated qualitatively with the Scherrer equation, by evaluating the peak width at half maximum.

2.10. Solid-state nuclear magnetic resonance spectroscopy (NMR) analysis

Solid state NMR spectra were collected using a Varian Unity INOVA spectrometer. Cross-Polarization Magic Angle Spinning (CP-MAS) 13 C – (1 H) experiments were performed at a field strength of 9.4 T using a resonance frequency of 100.529 MHz for 13 C and 399.760 MHz for 1 H

with a 4.0 mm Chemagnetics T3 probe and a spinning rate of 10 kHz. A Hahn echo was appended to the CP-MAS sequence with an echo delay of one rotor period. The ^{13}C 180° pulse of 5 μs was used for the echo. A ^{1}H 90° pulse of 3.3 μs and a constant amplitude spin lock pulse was used with a contact time of 2.0 ms, a ^{13}C radio frequency strength of 85 kHz and a ^{1}H radio frequency strength of 95 kHz. ^{1}H TPPM decoupling with a radio frequency strength of 100 kHz was used. All spectra were processed using the program RMN, version 2.01 (PhySy, Ltd., http://www.physyapps.com). The spectra were fit using a mixed gaussian/Lorentzian line shape in the DMFIT software suite [26]. All ^{13}C spectra were referenced to tetramethylsilane (0 ppm).

2.11. Statistical analysis

All statistical analysis was performed using GraphPad Prism 7. Normality of fiber diameter data was evaluated through a Shapiro-Wilk test. Statistical analysis of the cellulose yield, liquid absorption capabilities, and fiber diameter was conducted using an analysis of variance (ANOVA) followed by a Tukey post-hoc test. Statistical analysis of cell viability was conducted using Welch's t-test. All data are presented as mean \pm standard deviation (SD) unless otherwise indicated.

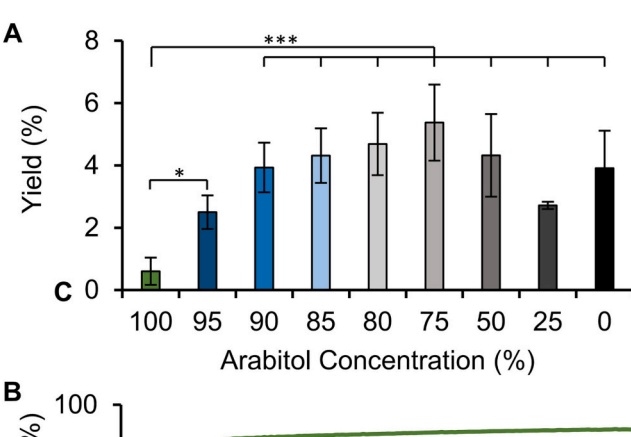
3. Results and discussion

3.1. BC yield and light transmittance

Commonly, K. hansenii is cultured using glucose as a carbon source. In this work, we tested BC production using different mixtures of progressively increased arabitol and decreased glucose content (Table 1). Pellicles from the 100% arabitol group exhibited a significantly decreased BC yield of 0.6% (Fig. 1A), with concomitant increased pellicle transparency (Fig. 1B, C). Increased BC yield with incremental increases in glucose concentration were observed starting with the 95% arabitol group and peaking with the 75% arabitol group, with a maximum BC yield of 5.4%. This indicates that the addition of glucose and its subsequent metabolism directly aided in increased BC production. However, for the 50% to 0% arabitol groups a decrease in BC yield is observed. Though outside of the scope of the current work, the changes in yield may be due to altered metabolic processes. For instance, the low yield for the 100% arabitol group may be due to additional metabolic steps for arabitol utilization and the increased energetic cost associated with metabolism through the PPP. The decreased BC yield at the higher glucose concentrations may be due to gluconic acid production during glucose metabolism. An increase in gluconic acid production would decrease the pH of the culture, preventing effective BC formation [27,28].

When looking at transparency, pellicles from the 0% arabitol group exhibited an average light transmission of $25\pm2\%$, while the pellicles from the 100% arabitol group exhibited light transmission of $89\pm7\%$ (Figs. 1B, C, S2A, B). For the mixed carbon source groups, a stepwise increase in light transmittance was observed between 0% and 80% arabitol (Fig. 1B). This trend plateaus for pellicles in the 80%, 85%, and 95% arabitol groups at 65–73% light transmittance. When the arabitol concentration was increased from 95% to 100%, the light transmission increased from 73 \pm 6% to 89 \pm 7%, likely due to the significant decrease in BC yield.

The images in Fig. 1C further emphasize the optical clarity of pellicles formed using 80% arabitol or higher. The increase in yield associated with consistently higher transmittance values for 80%–90% arabitol groups indicated that the transparency was not a result of lower cellulose production. To ensure that differences in thickness and hydration did not affect light transmittance through the pellicles, side-view images and estimated thickness calculations were compared for each group (Fig. S3A, B). The estimated pellicle thickness was consistent with the low BC yield observed with 100% arabitol group. For the other groups (95% through 0% arabitol) a correlation between decreasing



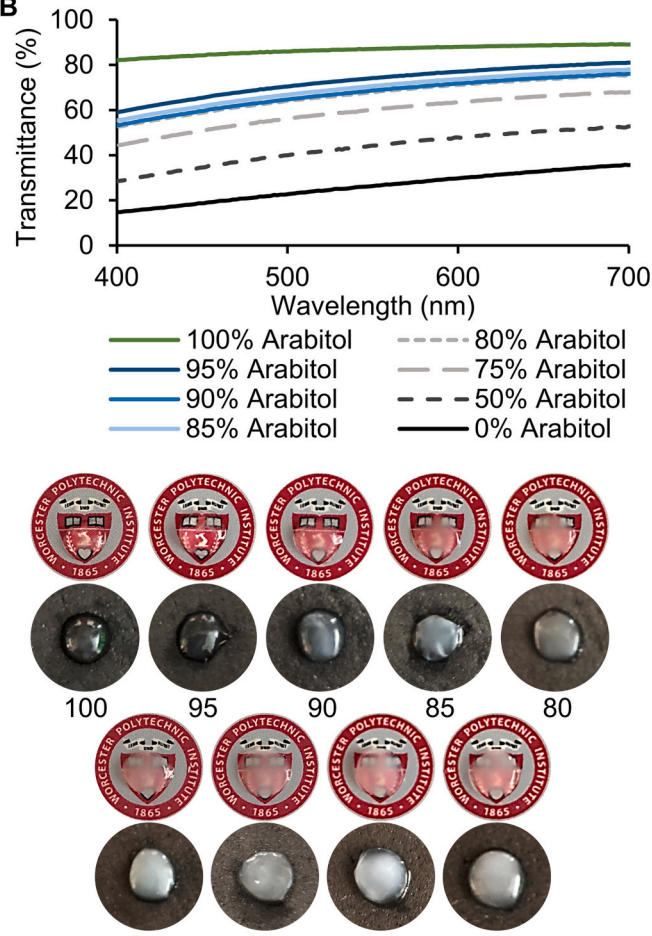


Fig. 1. Yield and light transmittance of BC produced by *K. hansenii* with varying arabitol concentrations. (A) BC yield from bacteria cultured with decreased arabitol concentrations. Data are presented as mean \pm SD from three independent experiments (n = 3 per experiment). Statistical differences determined by an ANOVA followed by the Tukey's HSD test (*p < 0.01, ***p < 0.001). (B) Increased transparency with increased arabitol concentrations shown through light transmission (C) and imaging.

50

transparency and increasing BC thickness was not observed. In addition to pellicle thickness, a qualitative assessment of pellicle handleability was performed (Fig. S4). For all groups other than 100% arabitol, no qualitative difference in handleability was observed (Videos S1–S5).

Compared to commercially available wound dressing, BC pellicles produced using arabitol exhibited transmission values between that of film based wound dressings, and hydrogel-based dressings. Polyurethane derived film wound dressings such as 3M Medical's TegadermTM and Johnson and Johnson's BioclusiveTM have light transmission values of 74.4% and 89.4%, respectively [29]. Though these wound

dressings exhibit higher transmission values than the BC produced using 80–95% arabitol, these dressings are only indicated for use as protective coverings of low exudating wounds. The Covidien $^{\rm TM}$ Kendall $^{\rm TM}$ PEG/propylene glycol derived hydrogel wound dressing exhibited a light transmission lower than the BC produced using 80–95% arabitol, with a transmission value of 53 \pm 1% (Fig. S2A, B). This hydrogel wound dressing is marketed as extremely absorbent while its transparency allows for wound visualization. Overall, these results indicate that BC pellicles produced using 80–95% arabitol exhibit transmittance values within the range of commercially available transparent wound dressings.

3.2. Bacterial growth kinetics

Growth kinetic experiments were performed to compare how each arabitol concentration group affected the growth rate of *K. hansenii*. From the growth kinetic curves (Fig. 2A), there was a delay in the onset of the exponential growth phase with increasing arabitol concentration. Using the slope of the linear region of the growth kinetic curves, maximum growth rate (μ_{max}) values were calculated (Fig. 2B). All arabitol groups tested resulted in comparable μ_{max} values ranging between 0.0050 and 0.0069 h⁻¹. No statistical significance was observed, indicating the arabitol concentration has little impact on the maximum growth rate of *K. hansenii*.

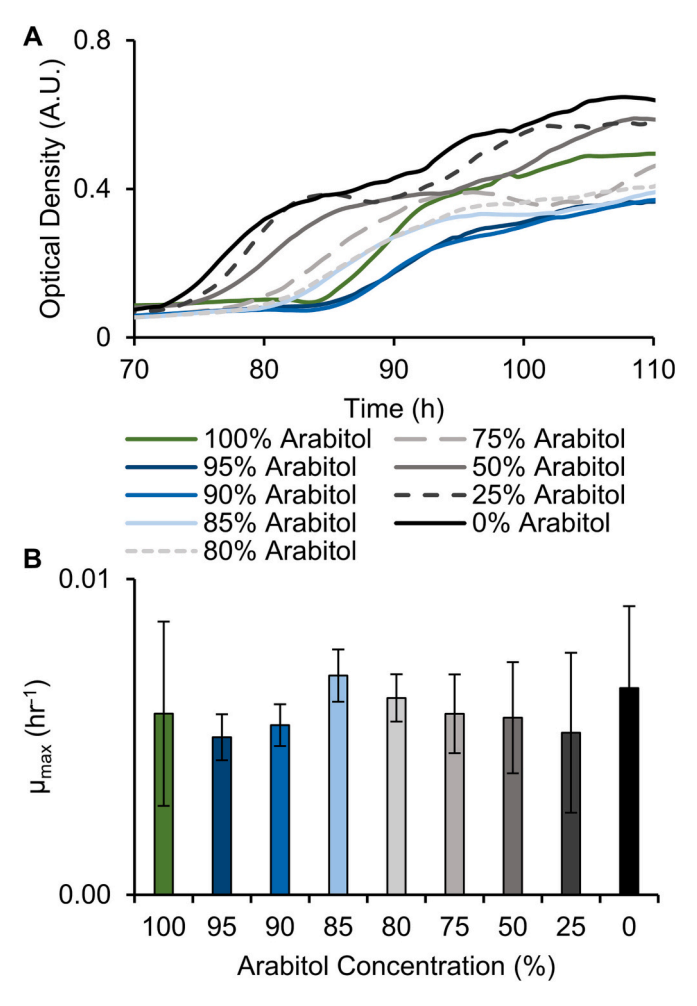


Fig. 2. K. hansenii bacterial growth using reduced amounts of arabitol. (A) Bacterial growth kinetics curves. (B) Maximum growth rate (μ_{max}) identified from the linear region of the growth kinetic curves. Data are presented as mean \pm SD from three independent experiments (n = 3 per arabitol concentration and experiment).

3.3. BC liquid absorption

To assess the effect of the culture condition on the intrinsic properties of the BC produced, liquid absorption analysis was performed. The liquid absorption capacity of freeze-dried BC pellicles 1 h (Fig. 3A) and 24 h (Fig. 3B) after initial submersion was assessed. No significant difference in liquid absorption was observed between 1 h and 24 h, indicating that pellicles had maximized liquid absorption by 1 h. At 1 h, a significant difference in liquid absorption was observed between the 0% arabitol control group and 95%, 90%, 85%, 80%, and 75% arabitol groups; where the 0% arabitol group had an average of 128-fold increase in mass, while 95%, 90%, 85%, 80%, and 75% arabitol groups had averages of 71, 58, 62, 52, and 50-fold mass increases, respectively. The region between 75% and 95% arabitol correlated to the transparency plateau identified in Fig. 1B. Similarly, at 24 h the 0% arabitol group had an average of 148-fold mass increase, while 95%, 90%, 85%, 80%, and 75% arabitol groups had an average of 69, 54, 65, 53, and 51-fold increase in mass, respectively (Fig. 3B). At both the 1 h and 24 h time points 100% arabitol BC pellicles absorbed more liquid, 108-fold and 111-fold increase in mass respectively, than pellicles produced using 75%–95% arabitol. The increase in liquid absorption capability of BC pellicles produced using 100% arabitol indicated that liquid absorption does not directly correlate with increased transparency. Previous research has reported a 37.3-fold mass increase for dry BC films [30]. However, a different Komagataeibacter strain was used to produce the pellicles, potentially leading to altered liquid absorption capabilities.

3.4. BC cytotoxicity

Viability of NHDF cells exposed to BC pellicles formed using 85% and 0% arabitol were assessed using a resazurin metabolic based colorimetric assay. Normalized to the untreated control, cell viability after exposure to BC formed using 85% and 0% arabitol was 71.4 \pm 7.4% and 82.6 \pm 14.1% respectively (Fig. S5A). No statistical difference in viability was observed, nor any changes to overall cell morphology (Fig. S5B).

3.5. BC fiber diameter

Since BC is produced as a semicrystalline nanofibrous network, it is possible that the fiber diameter may change due to altered carbon sources. To investigate if using glucose and arabitol as the carbon sources alter BC fiber diameter, SEM imaging and image analysis was performed. BC pellicles from the most transparent group (100% arabitol), the transparency plateau region (85% arabitol group), below the transparency plateau region (50% arabitol group), and the control (0% arabitol group) were evaluated (Fig. 4). Fiber diameter analysis indicated that the 100% arabitol group had an average median fiber diameter that was significantly larger than all other groups (52 nm versus 32–41 nm). Conversely, the 85% arabitol group had the smallest average median fiber diameter (32 nm), while 50% and 0% arabitol produced pellicles with average median fiber diameters of 41 nm and 39 nm, respectively. Though it may seem counter intuitive that 100% arabitol and 85% arabitol would produce pellicles with the largest and smallest fiber widths, respectively, an additional observation regarding fiber density was observed; the 85% arabitol group produced BC pellicles with a more dense (larger number of fibers) network structure as observed by SEM imaging (Fig. 4). Lower fiber density has been attributed to nutrient restriction in the media culture [9]; however, this reasoning does not apply in this case. The 100% arabitol group arguably provides a more nutrient restrictive media condition than 85% arabitol group given the lack of glucose present, and differences in fiber density were not observed between 100% arabitol and 0% arabitol. An alternative explanation may be attributed to how the bacterium produces cellulose. Cellulose fibers are extruded from the bacterium as 1.5 nmwide nanofibers that self-assemble in microfibril bundles [31,32]. SEM

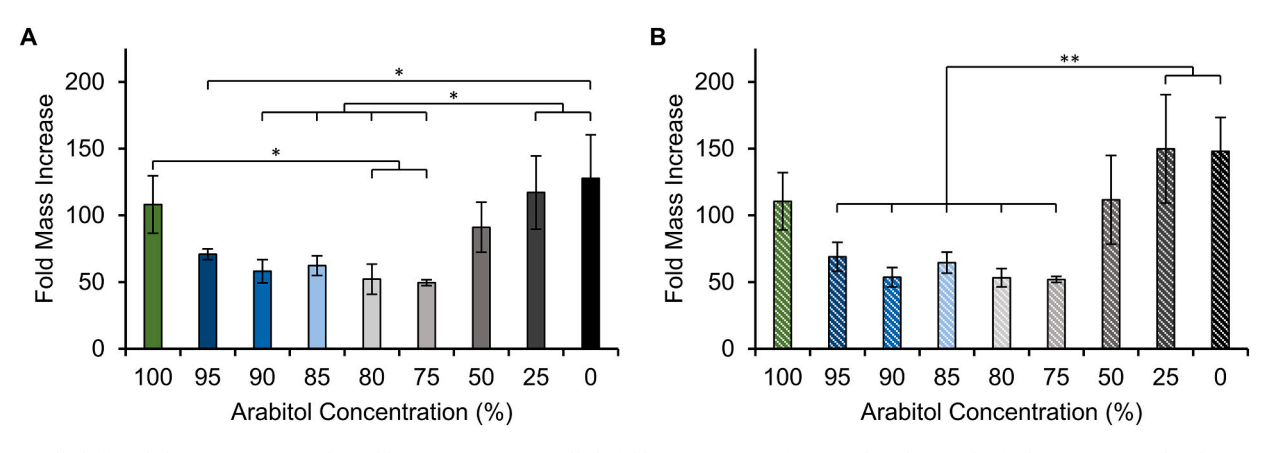


Fig. 3. BC pellicle liquid absorption presented as fold mass increase. BC pellicle fold mass increase after (A) 1 h and (B) 24 h of submersion in a salt solution. Data are presented as mean \pm SD from three independent experiments (n = 3 per experiment). Statistical differences determined by an ANOVA followed by the Tukey's HSD test (*p < 0.05, **p < 0.005).

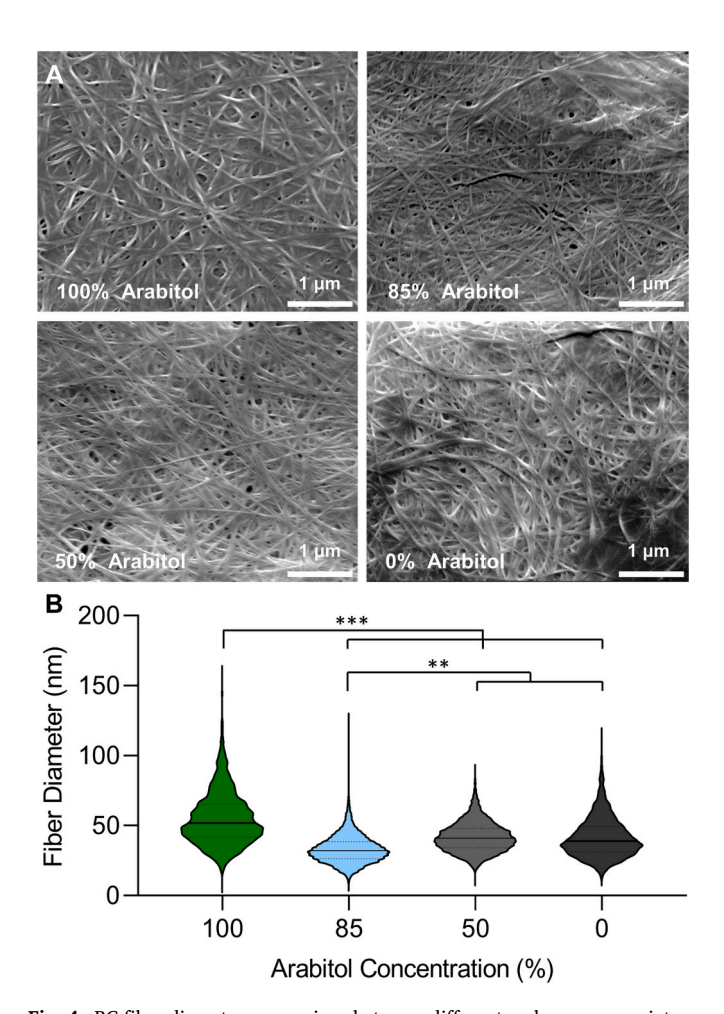


Fig. 4. BC fiber diameter comparison between different carbon source mixture groups. (A) SEM images at $30000\times$ of the microstructure and fiber morphology of BC pellicles. (B) BC nanofibril diameter values. Data are presented as median \pm SD from three independent experiments (n = 6 images per pellicle). Statistical differences determined by an ANOVA followed by the Tukey's HSD test (**p < 0.005, ***p < 0.0005).

imaging allows for the diameter measurement of the microfibril bundle and not the individual extruded nanofibers. The occurrence of more fibers with lower fiber diameter, as in the case for the 85% arabitol group, may indicate that the conformation or crystallization of the initial extruded nanofiber may be altered in a way that prevents extensive self-

assembly of the fibers post-extrusion.

3.6. SAXS analysis

Further characterization of the morphology was performed through analysis of SAXS spectra. As the percentage of arabitol used for BC production increased, the overall shape of the SAXS spectra and the features corresponding to large-scale structures were retained and no shoulder-like scattering was observed (Fig. 5A). A small feature was observed in the range $q=0.025-0.1~{\rm A}^{-1}$ (Fig. 5B). This feature manifests as two small peaks, corresponding to length scales of about 9.7 nm and 11.7 nm; the characteristic length scale is estimated at 2π over q. As the concentration of arabitol increased, these peaks gradually became broader and less prominent until they were nearly indistinguishable for the pellicle produced using 100% arabitol. Additionally, there appeared to be a slight variation in the slope of the decay of the scattered intensity at low q. This feature appeared to be minimal and retained across the groups, so further analysis would be needed to determine whether it corresponds to a subtle change in the structure.

Differences in the relative intensities likely do not occur due to a difference in scattering power (electron density) but in the relative pellicle densities in the X-ray path. The scattered intensity generally followed a power-law decay with an α exponent of 2 at very low q, then 2.6 at higher q. Though there was a slight deviation in the region where the features exist, these α exponent values are consistent with literature values of hydrated cellulose. Where low q regions ($<0.05~\text{Å}^{-1}$) corresponds to the inner structure of water swollen BC bundles while high q regions ($<0.07~\text{Å}^{-1}$) correspond to the surface of the BC pellicle plus a constant background [33–35]. BC pellicles are comprised of highly crystalline and amorphous regions that cannot be distinguished though SAXS analysis. Further crystallite dimension and crystalline fraction analysis was determined using WAXS and solid-state NMR.

3.7. WAXS and solid-state NMR analysis

Further characterization of the morphology and molecular structural differences between BC pellicles was performed via WAXS and solid-state NMR. When analyzing the pellicles via WAXS, the peak width at a 2θ value of 13.4 was fairly maintained across all groups, indicating that the crystallite size remained the same (Fig. 6). Though the peak width at a 2θ value of 13.4 was maintained, the peak intensity varied with changing arabitol concentration, even when adjusted to the scale of the scattering intensity. When comparing the ratio of the peak intensities with the total intensity of the spectra, there was a steady increase observed between 25% and 75% arabitol groups. Peak intensity was lost for the 80% arabitol group, and then slowly increases again between

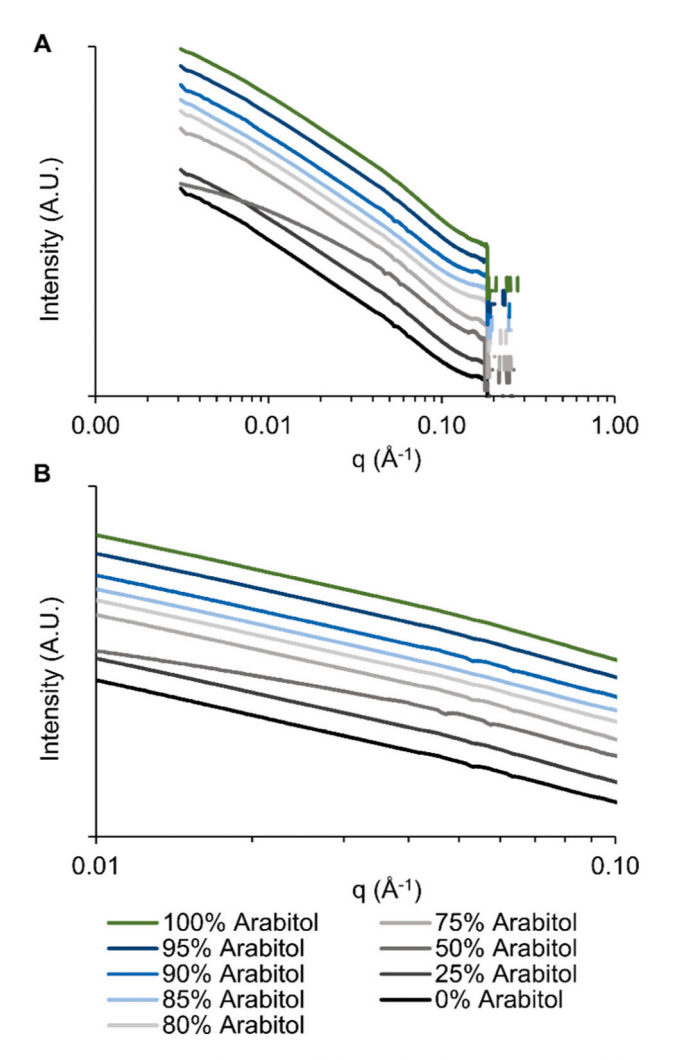


Fig. 5. SAXS intensities from BC pellicles produced using mixtures of glucose and arabitol. (A) Full spectral reading of each pellicle and (B) zoomed in identified region of interest.

85% arabitol and 95% arabitol groups and reached a maximum peak intensity for the 100% arabitol group. The loss in peak intensity for pellicles produced using 80% to 95% arabitol corresponds with the previously identified plateaued transparency and liquid absorption findings. The change in peak intensity could be attributed to a change in crystallinity. However, the broad peak between a 20 value of 15 and 20, which is likely due to water or possibly amorphous regions of the cellulose, prevents accurate crystallinity calculation [36]. Overall WAXS analysis showed that peak positions and the number of peaks were wellmaintained across all groups, indicating the crystal phase was not affected.

To further analyze the crystallinity of the pellicles produced, solid state CP-MAS NMR analysis was performed (Fig. 7). To properly compare spectra between groups of interest, CP-MAS NMR was performed on a group selected based the transparency data: (1) group above the transparent plateau region (100% arabitol), (2 and 3) groups within and directly below the plateau region (85% arabitol and 75% arabitol), (4) well below the plateau region (50% arabitol and 25% arabitol), and (5) the control group (0% arabitol). Full spectra between 0 and 250 ppm were collected (Fig. 7A), and the region corresponding to cellulose structure was isolated between 50 and 110 ppm (Fig. 7B). To quantify the relative crystallinity of the pellicles, the crystalline and amorphous regions of the resonances at the C-4 carbon in the BC pellicles were fit primarily with one gaussian peak each. This was done by fitting a gaussian peak for the crystalline region centered around 88 ppm and a

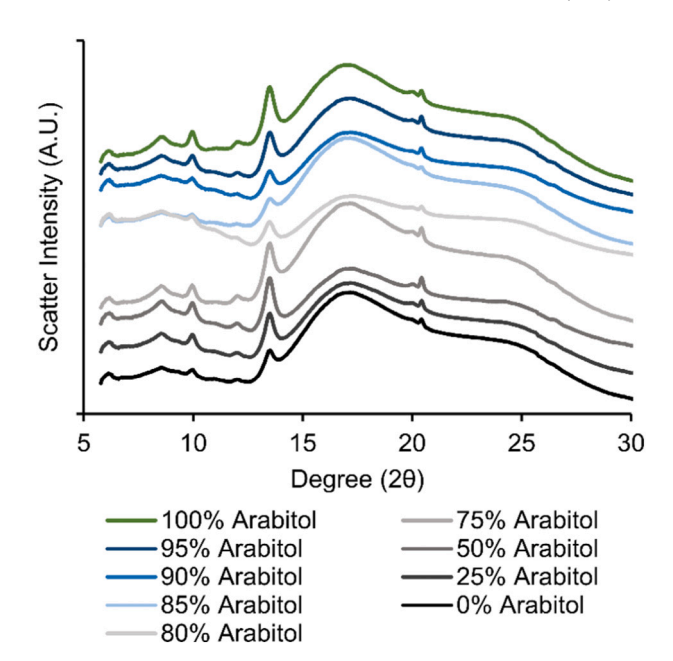


Fig. 6. WAXS intensities from BC pellicles produced using mixtures of glucose and arabitol.

gaussian peak for the amorphous region centered around 84 ppm. A small additional gaussian peak was included where necessary to better replicate the line shape; in most cases this line belonged in the amorphous region of the signal. Additional gaussian fits were used to build out the other regions of the ¹³C NMR signal to allow for a proper fit of the region of interest using least-squares difference minimization. To determine the areas of the crystalline and amorphous regions of the C-4 signal, two approaches were utilized: 1) areas of the fitted peak shapes and 2) integrated areas of the two regions sans fitting. For both calculation methods, the same trends were observed, and no appreciable crystallinity differences were observed between arabitol concentration groups (Table 2). The crystallinity observed in this study is lower than some of the values previously reported [37–39]. However, culture conditions such as temperature, specific strain, and media pH are known to alter crystallinity so direct comparisons are not always accurate [32].

When the overall spectrum for the pellicles was considered (Fig. 7A), a difference was observed in the total amount of cellulose in the pellicle. In all groups, a signal for a carboxylic acid group (-COOH) at around 172 ppm was observed (Fig. 7C). The intensity of this peak varied slightly from group to group. A second set of signals were observed in the 110 to 160 ppm region that was associated with aromatic carbons. These signals also manifested spinning side bands at the expected multiples of the magic angle spinning rate, 10 kHz, indicative of the order and crystallinity of these carbon atoms. Using the integrated region of the C-1 carbon signal of cellulose at 105 ppm and the integrated regions of the aromatic carbons, an estimate of the percentage of aromatic carbons was calculated. In the case of aromatic carbons, the overall integral was summed from the primary chemical shift region along with the side band regions. The overall integral for the aromatic carbons was divided by six for the purpose of population estimation. The overall aromatic carbon content was found to vary across the groups. Both cellulose and aromatic carbon structures were observed in the 0% arabitol group. The aromatic carbon content decreased in the 25% arabitol group as compared to the 0% arabitol group. The 50% and 75% arabitol group exhibited no aromatic carbons potentially due to the strong signal contributed by the C1-C6 carbons. The cross-polarization conditions used across samples were the same and the observed level of crystallinity in the cellulose component was constant, so the efficiency of the CP-MAS NMR is expected to be the same for each experiment. The difference in observed signal intensities would then be governed essentially by carbon

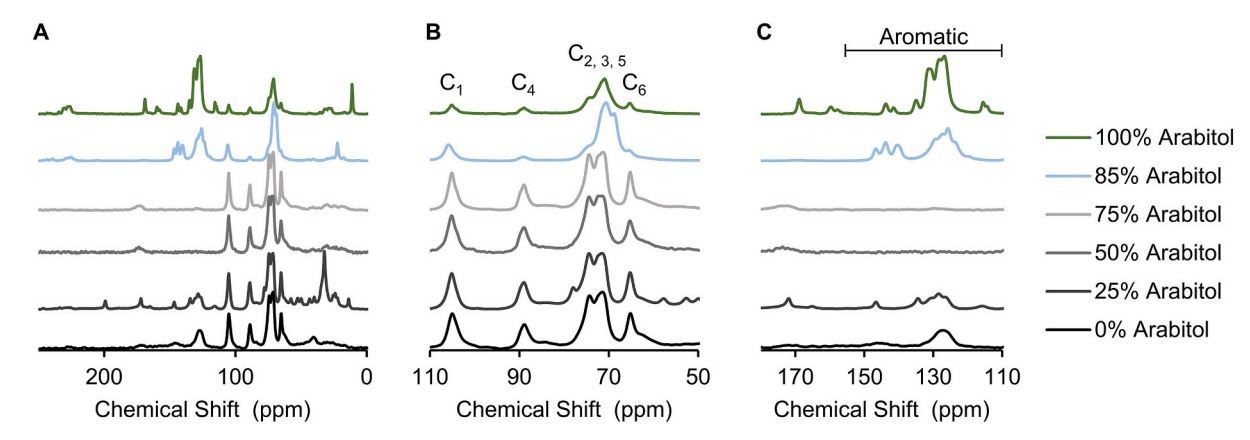


Fig. 7. CP-MAS spectra of BC produced using various carbon source mixtures. (A) Variation in full NMR spectra of BC pellicles, (B) spectra associated with the cellulose molecular region (the peaks for the C_{1-6} carbons are identified), and (C) isolated region attributed to aromatic carbons in the pellicles.

 Table 2

 Cellulose crystallinity relative to arabitol concentration.

Arabitol concentration (%)	Crystallinity (% by peak fit method)	Crystallinity (% by integration method)
100	70	66
85	69	65
75	65	67
50	68	65
25	66	65
0	70	61

content. As the 50% arabitol and 75% arabitol groups resulted in pellicles with higher yields, it is possible that the aromatic signatures are present but undetectable due to their relative abundance in the sample. Subsequently, the aromatic carbons appeared in the 85% and 100% arabitol group. For the 100% arabitol group, the aromatic carbons made up most of the carbon fraction by an approximate factor of four. Though the presence of aromatic carbons in BC has not been reported previously, it is known that the polymers produced by these bacterium can be influenced by culture conditions [40].

Though the predominant insoluble exopolysaccharide produced by this class of microbes is cellulose, other exopolysaccharides have been reported when grown on alternative carbon sources [41–44]. The bacterial cellulose synthases of *Acetobacter* species have previously been shown to be promiscuous – Yadav et al. showed that UDP-GlcNAc could be incorporated into the BC polymer chain [43]. Additionally, other exopolysaccharides have been reported when grown on alternative carbon sources [41–44]. It is plausible that other UDP-sugars are formed under the conditions reported here and incorporated into the exopolysaccharide giving rise to the differences observed in the cellulose molecular region of the NMR.

The aromatic signature is most likely from proteinaceous extracellular material, which is often found in naturally derived biopolymers. Further evidence for this is that the aromatic signature is anticorrelated with BC yield - essentially, protein may make up a higher fraction of the pellicle when BC yield is lower. Williams et al. showed that aromatic amino acids, such as phenylalanine, tryptophane, and tyrosine exhibit ¹³C signal between 100 and 160 ppm [45]. These aromatic amino acids are formed in both the PPP and glycolysis [46]. The surprising observation of these proteinaceous aromatic signatures in both the 0% and 100% arabitol groups could be attributed to underrepresentation of BC ¹³C NMR signal ranges than 100 ppm, alternative allocation of increased signal in the 100-160 ppm range, and differences in bacterial strains researched. 13C NMR signal for BC is predominantly truncated to show signal only within the 50–110 ppm range, resulting in underreporting of regions outside of the cellulose range [47,48]. Alternatively, Yamazawa et al., attributed signal in the aromatic region to the presence of spinning

sidebands [49]. Further, the reclassification of *K. hansenii* as the proposed representative type strain for a new genus (*Novacetimonas*) based on phylogenetic analysis of the cellulose biosynthesis genes, indicated that there are distinct genetic differences from other *Komagataeibacter* strains [50], which may produce distinctly different exopolymers and concentration of proteinaceous extracellular material. The exact chemical composition of the exopolymers present within the pellicles using blends of glucose and arabitol as the carbon source is subject of continued investigation.

4. Conclusions

In this study, a method was developed to produce novel tunable transparent bacterial-derived cellulose. It was determined that modulation of the ratio of glucose and arabitol as the carbon source in static culture aided in the production of transparent BC by K. hansenii. Similar trends in data convergence for higher arabitol concentration groups (80%-95%), were observed for transparency, liquid absorption capabilities, and WAXS spectra analysis. A significantly smaller fiber diameter was also observed in the 85% arabitol group. Overall, these observations indicate that the use of arabitol concentrations between 80% and 95%, while holding mass of carbon-containing species constant, results in changes to both the microstructures and molecular structures of the BC produced. BC produced using higher arabitol concentrations (between 75%-95%) exhibited average transmittance values >60%, while 100% arabitol group pellicles allowed for over 80% transmittance. Overall, the 85% arabitol group produced optimal pellicles based on the balance between cellulose yield and material transparency. Though the mechanism for this increased transparency was determined to not be due to decreased crystallinity, NMR spectra revealed a shift in sugar carbon signals and an aromatic signature that is strongest in the 100% arabitol group. This result indicates that K. hansenii NQ5 may not solely produce pure BC when supplemented with arabitol. This work is the first to show that BC composition and transparency can be manipulated by carbon source alone. This establishes that new exopolymers of varying monomer composition may be accessible simply through the feeding of Komagataeibacter species with different carbon sources.

CRediT authorship contribution statement

Elizabeth M. van Zyl: Conceptualization, Methodology, Formal analysis, Investigation, Writing – original draft, Visualization, Writing – review & editing. **Mitchell A. Kennedy:** Methodology, Writing – original draft, Investigation, Formal analysis. **Wendy Nason:** Methodology, Investigation, Formal analysis. **Sawyer J. Fenlon:** Validation, Writing – review & editing. **Eric M. Young:** Conceptualization, Methodology,

Writing – review & editing. Luis J. Smith: Conceptualization, Methodology, Formal analysis, Resources, Writing – original draft, Writing – review & editing. Surita R. Bhatia: Conceptualization, Methodology, Formal analysis, Resources, Writing – review & editing. Jeannine M. Coburn: Conceptualization, Methodology, Formal analysis, Investigation, Writing – review & editing, Supervision, Visualization, Project administration.

Declaration of competing interest

The authors declare the following financial interests/personal relationships which may be considered as potential competing interests: Jeannine M. Coburn, Elizabeth M. van Zyl, and Eric M. Young have the patent Transparent Cellulose-Based Materials and Methods of Making the Same pending to Worcester Polytechnic Institute.

Data availability

Data will be made available on request.

Acknowledgments

This research used resources of the Electron Microscopy Core Facility at UMass Chan Medical School supported by Award Number S10RR021043 from the National Institutes of Health National Center for Research Resources. This research used beamline 11-BM of the National Synchrotron Light Source II, U.S. Department of Energy (DOE) Office of Science User Facilities operated for the DOE Office of Science by Brookhaven National Laboratory under Contract No. DE-SC0012704. We thank Dr. Ruipeng Li, Brookhaven National Laboratory, for the SAXS/WAXS measurements. We thank Dr. David Dolivo for his critical feedback and review of this manuscript. Support for MAK was provided by the National Science Foundation awards DGE-1922639 and DMR-1905547. This research was supported in part by with funding from the WPI Dean of Engineering Seed Fund to JMC and EMY.

Appendix A. Supplementary data

Supplementary data to this article can be found online at https://doi.org/10.1016/j.bioadv.2023.213345.

References

- [1] S.-P. Lin, H.-N. Kung, Y.-S. Tsai, T.-N. Tseng, K.-D. Hsu, K.-C. Cheng, Novel dextran modified bacterial cellulose hydrogel accelerating cutaneous wound healing, Cellulose 24 (11) (2017) 4927–4937.
- [2] A. Gupta, S.M. Briffa, S. Swingler, H. Gibson, V. Kannappan, G. Adamus, I. Radecka, Synthesis of silver nanoparticles using curcumin-cyclodextrins loaded into bacterial cellulose-based hydrogels for wound dressing applications, Biomacromolecules 21 (2020) 1802–1811.
- [3] A. Gupta, D. Keddie, V. Kannappan, H. Gibson, I. Khalil, M. Kowalczuk, I. Radecka, Production and characterisation of bacterial cellulose hydrogels loaded with curcumin encapsulated in cyclodextrins as wound dressings, Eur. Polym. J. 118 (2019) 437–450.
- [4] M.J. Tabaii, G. Emtiazi, Transparent nontoxic antibacterial wound dressing based on silver nano particle/bacterial cellulose nano composite synthesized in the presence of tripolyphosphate, J. Drug Deliv. Sci. Technol. 44 (2018) 244–253.
- [5] Z. Di, Z. Shi, M.W. Ullah, S. Li, G. Yang, A transparent wound dressing based on bacterial cellulose whisker and poly (2-hydroxyethyl methacrylate), Int. J. Biol. Macromol. 105 (2017) 638–644.
- [6] Y. Wang, C. Wang, Y. Xie, Y. Yang, Y. Zheng, H. Meng, K. Qiao, Highly transparent, highly flexible composite membrane with multiple antimicrobial effects used for promoting wound healing, Carbohydr. Polym. 222 (2019), 114985.
- [7] H. Kono, H. Tsujisaki, K. Tajima, Reinforcing poly (methyl methacrylate) with bacterial cellulose nanofibers chemically modified with methacryolyl groups, Nanomaterials 12 (3) (2022) 537.
- [8] F.G. Torres, O.P. Troncoso, K.N. Gonzales, R.M. Sari, S. Gea, Bacterial cellulose-based biosensors, Med. Dev. Sensors 3 (5) (2020), e10102.
 [9] S.S. de Souza, F.V. Berti, K.P. de Oliveira, C.Q. Pittella, J.V. de Castro, C. Pelissari,
- [9] S.S. de Souza, F.V. Berti, K.P. de Oliveira, C.Q. Pittella, J.V. de Castro, C. Pelissari, L.M. Porto, Nanocellulose biosynthesis by komagataeibacter hansenii in a defined minimal culture medium, Cellulose 26 (3) (2019) 1641–1655.

- [10] S. Wang, T. Li, C. Chen, W. Kong, S. Zhu, J. Dai, T. Li, Transparent, anisotropic biofilm with aligned bacterial cellulose nanofibers, Adv. Funct. Mater. 28 (24) (2018) 1707491.
- [11] N. Yin, M.D. Stilwell, T.M. Santos, H. Wang, D.B. Weibel, Agarose particle-templated porous bacterial cellulose and its application in cartilage growth in vitro, Acta Biomater. 12 (2015) 129–138.
- [12] K.V.S. Hodel, L.M.D.S. Fonseca, I.M.D.S. Santos, J.C. Cerqueira, R.E.D. Santos-Júnior, S.B. Nunes, B.A.S. Machado, Evaluation of different methods for cultivating Gluconacetobacter hansenii for bacterial cellulose and montmorillonite biocomposite production: wound-dressing applications, Polymers 12 (2) (2020) 267.
- [13] P. Zikmanis, S. Kolesovs, M. Ruklisha, P. Semjonovs, Production of bacterial cellulose from glycerol: the current state and perspectives, Bioresour. Bioprocess. 8 (1) (2021) 1–14.
- [14] S. Bandyopadhyay, N. Saha, P. Sáha, Characterization of bacterial cellulose produced using media containing waste apple juice, Appl. Biochem. Microbiol. 54 (6) (2018) 649–657.
- [15] Z. Hussain, W. Sajjad, T. Khan, F. Wahid, Production of bacterial cellulose from industrial wastes: a review, Cellulose 26 (5) (2019) 2895–2911.
- [16] M. Salari, M.S. Khiabani, R.R. Mokarram, B. Ghanbarzadeh, H.S. Kafil, Preparation and characterization of cellulose nanocrystals from bacterial cellulose produced in sugar beet molasses and cheese whey media, Int. J. Biol. Macromol. 122 (2019) 280–288
- [17] R.T. Machado, A.B. Meneguin, R.M. Sabio, D.F. Franco, S.G. Antonio, J. Gutierrez, S.C. Lazarini, Komagataeibacter rhaeticus grown in sugarcane molasses-supplemented culture medium as a strategy for enhancing bacterial cellulose production, Ind. Crop. Prod. 122 (2018) 637–646.
- [18] S.M. Keshk, K. Sameshima, Evaluation of different carbon sources for bacterial cellulose production, Afr. J. Biotechnol. 4 (6) (2005) 478–482.
- [19] T. Oikawa, T. Morino, M. Ameyama, Production of cellulose from D-arabitol by acetobacter xylinum KU-1, Biosci. Biotechnol. Biochem. 59 (8) (1995) 1564–1565.
- [20] A. Riley, Basics of polymer chemistry for packaging materials, in: Packaging Technology, Elsevier, 2012, pp. 262–286.
- [21] T. Oikawa, J. Nakai, Y. Tsukagawa, K. Soda, A novel type of D-mannitol dehydrogenase from acetobacter xylinum: occurrence, purification, and basic properties, Biosci. Biotechnol. Biochem. 61 (10) (1997) 1778–1782.
- [22] M. Rezazadeh, V. Babaeipour, E. Motamedian, Reconstruction, verification and insilico analysis of a genome-scale metabolic model of bacterial cellulose producing Komagataeibacter xylinus, Bioprocess Biosyst. Eng. (2020) 1–10.
- [23] S.S.D. Souza, J.D.V. Castro, L.M. Porto, Modeling the core metabolism of Komagataeibacter hansenii ATCC 23769 to evaluate nanocellulose biosynthesis, Braz. J. Chem. Eng. 35 (2018) 869–886.
- [24] M. Gullo, S. La China, G. Petroni, S. Di Gregorio, P. Giudici, Exploring K2G30 genome: a high bacterial cellulose producing strain in glucose and mannitol based media, Front. Microbiol. 10 (2019) 58.
- [25] K.-Y. Lee, J.J. Blaker, A. Bismarck, Surface functionalisation of bacterial cellulose as the route to produce green polylactide nanocomposites with improved properties, Compos. Sci. Technol. 69 (15–16) (2009) 2724–2733.
- [26] D. Massiot, F. Fayon, M. Capron, I. King, S. Le Calvé, B. Alonso, G. Hoatson, Modelling one-and two-dimensional solid-state NMR spectra, Magn. Reson. Chem. 40 (1) (2002) 70–76.
- [27] K. Toda, T. Asakura, M. Fukaya, E. Entani, Y. Kawamura, Cellulose production by acetic acid-resistant Acetobacter xylinum, J. Ferment. Bioeng. 84 (3) (1997) 228–231.
- [28] C. Zhong, G.-C. Zhang, M. Liu, X.-T. Zheng, P.-P. Han, S.-R. Jia, Metabolic flux analysis of Gluconacetobacter xylinus for bacterial cellulose production, Appl. Microbiol. Biotechnol. 97 (14) (2013) 6189–6199.
- [29] C. Chen, D.G. Diven, S. Lockhart, B. Bell, Laser transmission through transparent membranes used in cutaneous laser treatment, J. Am. Acad. Dermatol. 45 (6) (2001) 919–923.
- [30] B. Wei, G. Yang, F. Hong, Preparation and evaluation of a kind of bacterial cellulose dry films with antibacterial properties, Carbohydr. Polym. 84 (1) (2011) 533–538.
- [31] R.M. Brown Jr., J. Willison, C.L. Richardson, Cellulose biosynthesis in acetobacter xylinum: visualization of the site of synthesis and direct measurement of the in vivo process, Proc. Natl. Acad. Sci. 73 (12) (1976) 4565–4569.
- [32] E.M. van Zyl, J.M. Coburn, Hierarchical structure of bacterial-derived cellulose and its impact on biomedical applications, Curr. Opin. Chem. Eng. 24 (2019) 122–130.
- [33] P.A. Penttilä, T. Imai, M. Capron, M. Mizuno, Y. Amano, R. Schweins, J. Sugiyama, Multimethod approach to understand the assembly of cellulose fibrils in the biosynthesis of bacterial cellulose, Cellulose 25 (5) (2018) 2771–2783.
- [34] P.A. Penttilä, T. Imai, J. Sugiyama, Fibrillar assembly of bacterial cellulose in the presence of wood-based hemicelluloses, Int. J. Biol. Macromol. 102 (2017) 111–118.
- [35] P.W. Schmidt, Small-angle scattering studies of disordered, porous and fractal systems, J. Appl. Crystallogr. 24 (5) (1991) 414–435.
- [36] A. Kamdem Tamo, I. Doench, L. Walter, A. Montembault, G. Sudre, L. David, A. Bernstein, Development of bioinspired functional chitosan/cellulose nanofiber 3D hydrogel constructs by 3D printing for application in the engineering of mechanically demanding tissues, Polymers (Basel) 13 (10) (2021) 1663.
- [37] W. Czaja, D. Romanovicz, R. Malcolm Brown, Structural investigations of microbial cellulose produced in stationary and agitated culture, Cellulose 11 (3–4) (2004) 403–411.
- [38] S. Sheykhnazari, T. Tabarsa, A. Ashori, A. Shakeri, M. Golalipour, Bacterial synthesized cellulose nanofibers; effects of growth times and culture mediums on the structural characteristics, Carbohydr. Polym. 86 (3) (2011) 1187–1191.

- [39] P. Singhsa, R. Narain, H. Manuspiya, Physical structure variations of bacterial cellulose produced by different komagataeibacter xylinus strains and carbon sources in static and agitated conditions, Cellulose 25 (3) (2018) 1571–1581.
- [40] J. Trček, I. Dogsa, T. Accetto, D. Stopar, Acetan and acetan-like polysaccharides: genetics, biosynthesis, structure, and viscoelasticity, Polymers 13 (5) (2021) 815.
- [41] L. Fang, J.M. Catchmark, Characterization of cellulose and other exopolysaccharides produced from gluconacetobacter strains, Carbohydr. Polym. 115 (2015) 663–669.
- [42] V. Yadav, B. Panilaitis, H. Shi, K. Numuta, K. Lee, D.L. Kaplan, N-acetylglucosamine 6-phosphate deacetylase (nagA) is required for N-acetyl glucosamine assimilation in gluconacetobacter xylinus, PLoS One 6 (6) (2011), e18099.
- [43] V. Yadav, B.J. Paniliatis, H. Shi, K. Lee, P. Cebe, D.L. Kaplan, Novel in vivodegradable cellulose-chitin copolymer from metabolically engineered gluconacetobacter xylinus, Appl. Environ. Microbiol. 76 (18) (2010) 6257–6265.
- [44] V. Yadav, L. Sun, B. Panilaitis, D.L. Kaplan, In vitro chondrogenesis with lysozyme susceptible bacterial cellulose as a scaffold, J. Tissue Eng. Regen. Med. 9 (12) (2015) E276–E288.

- [45] J.K. Williams, K. Schmidt-Rohr, M. Hong, Aromatic spectral editing techniques for magic-angle-spinning solid-state NMR spectroscopy of uniformly 13C-labeled proteins, Solid State Nucl. Magn. Reson. 72 (2015) 118–126.
- [46] K. Shimizu, Bacterial Cellular Metabolic Systems: Metabolic Regulation of a Cell System with 13C-metabolic Flux Analysis, Elsevier, 2013.
- [47] A. Idström, S. Schantz, J. Sundberg, B.F. Chmelka, P. Gatenholm, L. Nordstierna, 13C NMR assignments of regenerated cellulose from solid-state 2D NMR spectroscopy, Carbohydr. Polym. 151 (2016) 480–487.
- [48] J.-S. Jeong, J.-Y. Park, Water absorption and maintenance of nanofiber cellulose production by Gluconacetobacter rhaeticus TL-2C, Afr. J. Biotechnol. 11 (40) (2012) 9630–9632.
- [49] A. Yamazawa, T. Iikura, A. Shino, Y. Date, J. Kikuchi, Solid-, solution-, and gasstate NMR monitoring of 13C-cellulose degradation in an anaerobic microbial ecosystem, Molecules 18 (8) (2013) 9021–9033.
- [50] P.R. Brandão, M.T. Crespo, F.X. Nascimento, Phylogenomic and comparative analyses support the reclassification of several Komagataeibacter species as novel members of the Novacetimonas gen. nov. and bring new insights into the evolution of cellulose synthase genes, Int. J. Syst. Evol. Microbiol. 72 (2) (2022), 005252.